

Antiferromagnetic anisotropy determination by spin Hall magnetoresistance

Hua Wang,^{1,2,3} Dazhi Hou,^{4,*} Zhiyong Qiu,⁴ Takashi Kikkawa,^{3,4} Eiji Saitoh,^{3,4,5} and Xiaofeng Jin^{1,2}

¹State Key Laboratory of Surface Physics and Department of Physics, Fudan University, Shanghai 200433, China

²Collaborative Innovation Center of Advanced Microstructures, Fudan University, Shanghai 200433, China

³Institute for Materials Research, Tohoku University, Sendai 980-8577, Japan

⁴WPI Advanced Institute for Materials Research, Tohoku University, Sendai 980-8577, Japan

⁵Advanced Science Research Center, Japan Atomic Energy Agency, Tokai 319-1195, Japan

(Dated: February 28, 2018)

An electric method for measuring magnetic anisotropy in antiferromagnetic insulators (AFI) is proposed. When a metallic film with strong spin-orbit interaction, e.g. platinum (Pt), is deposited on an AFI, its resistance should be affected by the direction of the AFI Néel vector due to the spin Hall magnetoresistance (SMR). Accordingly, the direction of the AFI Néel vector, which is affected by both the external magnetic field and the magnetic anisotropy, is reflected in resistance of Pt. The magnetic field angle dependence of the resistance of Pt on AFI is calculated by considering the SMR, which indicates that the antiferromagnetic anisotropy can be obtained experimentally by monitoring the Pt resistance in strong magnetic fields. Calculations are performed for realistic systems such as Pt/Cr₂O₃, Pt/NiO and Pt/CoO.

I. INTRODUCTION

Antiferromagnetic materials, which were passively used to pin the magnetization of the adjacent magnetic layer through exchange bias, have now been gaining renewed attention due to the emerging antiferromagnetic spintronics.¹⁻¹⁴ Recently, the realization of all electric writing and readout antiferromagnetic (AFM) solid-state memory shows the efficient approach for manipulating AFM moments,⁸ which is well beyond the previous experimental investigation of anisotropic magnetoresistance (AMR) in AFMs,^{9,10} and indicates the potential broad application prospects in AFM recording media. Since low power consumption is also an important index for the ultrahigh-density integrated circuit,¹¹ one category of AFM materials, antiferromagnetic insulator (AFI), free of the charge current induced Joule heating because of its insulating nature, appear as promising candidates for future spintronics applications.^{2-6,12} Toward the practical application of AFI, it is of fundamental importance to obtain the AFI magnetic anisotropy as it defines the orientation of the Néel vector $\mathbf{\Delta} = \mathbf{M}_A/M_A - \mathbf{M}_B/M_B$. Owing to the difficulty for *ab initio* calculation of the magnetic anisotropy,¹⁵ experimental measurement provides a unique perspective for the investigation of magnetic anisotropy.

In analogy to the anisotropy determination in ferromagnets, the key point of measuring the antiferromagnetic anisotropy is monitoring the Néel vector direction under different external magnetic field directions. Generally, the standard approach for probing AFM Néel vector is X-ray magnetic linear dichroism (XMLD) measurement. For the determination of antiferromagnetic anisotropy, several methods are available based on the fitting results including AMR,^{16,17} magnetic torque,¹⁸ antiferromagnetic resonance (AFMR),¹⁹ Mossbauer spectral^{20,21} and muon spin relaxation (μ SR)²¹ study. These methods may work well for AFI bulk materials, however, the measurement usually gets challenging

for thin film samples which yield weak signals. Is there any convenient method for the Néel vector and anisotropy determination in both AFI bulk material and thin films?

Lately, a new type of magnetoresistance (MR) in a normal metal (NM)/ferromagnetic insulator (FI) bilayer systems, so-called spin Hall magnetoresistance (SMR), has drawn intense experimental^{4,22} and theoretical²³⁻²⁵ interest. The characteristic of the SMR is that it only depends on the interplay between electron spin polarization σ at the NM/FI interface and the magnetization \mathbf{M} of FI layer. The SMR, which is defined by the difference of the resistivity for magnetization \mathbf{M} perpendicular (ρ_{\perp}) and parallel (ρ_{\parallel}) to the current \mathbf{J}_C , can be formulated as $\rho_{\text{SMR}} = \rho_{\parallel} - \rho_{\perp}$. Since SMR measurement in NM/FI bilayers can directly tell the axis of magnetization \mathbf{M} of FI layer without distinguishing the inversion of the magnetization,²³⁻²⁵ it should be able to determine the antiferromagnetic Néel vector in a NM/AFI bilayer as well. Besides, in various AFI spintronics experiments, the investigation of spin current transport and SMR when inserting AFI NiO⁴⁻⁶ or CoO^{6,12} between Pt and YIG, indicate the strong interaction between the electron spin polarization σ and the AFI Néel vector $\mathbf{\Delta}$.

In this letter, we calculated SMR in Pt grown on Cr₂O₃(110), CoO(001) and NiO(001) thin films when rotating the external magnetic field in the film plane. The Néel vector angle versus external magnetic field direction at different magnetic field magnitudes were investigated systematically. For the uniaxial AFI Cr₂O₃, the external field direction dependence of SMR shows different symmetry for magnetic fields below and above the spin-flop field. While for the biaxial AFI NiO and CoO, the external field direction dependence of SMR was only simulated at the magnetic field magnitude higher than the spin-flop field, since even in the single crystal NiO and CoO, there naturally exist two equivalent inplane magnetic domains.^{26,27} Meanwhile, we successfully reproduced the anisotropy constant in uniaxial AFI Cr₂O₃ by fitting the SMR simulation curve only with the ex-

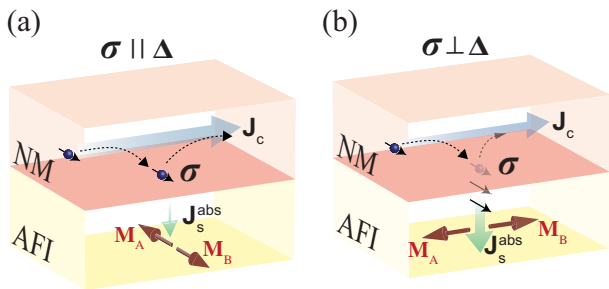


FIG. 1. (a), (b) Illustrations of the spin Hall magnetoresistance (SMR) in NM (NM=Pt)/AFI (AFI=Cr₂O₃, NiO, CoO) bilayer with AFI Néel vector parallel and perpendicular to the direction of the interface electron spin accumulation. \mathbf{J}_C and $\mathbf{J}_S^{\text{abs}}$ represent the injected charge current and the spin current absorption in AFI, respectively. \mathbf{M}_A and \mathbf{M}_B are the AFI sublattices.

perimental perpendicular susceptibility (which could also be obtained through the first-principle calculation values of exchange interaction constant). This work provides a versatile method to determine the Néel vector and anisotropy constant for both AFI bulk material and thin films.

II. SMR IN NM/AFI BILAYER

Let us consider a NM/AFI bilayer system when an electric current is applied in the Pt film, due to the spin Hall effect (SHE), the charge current will be converted into a spin current $\mathbf{J}_S = \theta_{\text{SH}}(\hbar/2e)\mathbf{J}_C \times \boldsymbol{\sigma}$ with spin polarization $\boldsymbol{\sigma}$ perpendicular to the electric current \mathbf{J}_C .^{28–30} The spin current with spin polarization $\boldsymbol{\sigma}$ parallel to the film surface is reflected back and gives rise to an induced charge current due to the inverse spin Hall effect (ISHE),^{22,31} as shown in Figs. 1(a) and (b). In analogy to the SMR in NM/FI, in NM/AFI bilayers, when electron spin polarization $\boldsymbol{\sigma}$ and Néel vector $\boldsymbol{\Delta}$ are not parallel, spin-flip scattering is activated. Figure 1(b) shows when $\boldsymbol{\sigma}$ and $\boldsymbol{\Delta}$ are perpendicular ($\mathbf{J}_C \parallel \boldsymbol{\Delta}$), the spin-transfer torque induced absorption at the NM/AFI interface will be maximized, which gives a higher resistance than the state $\mathbf{J}_C \perp \boldsymbol{\Delta}$. And the conductivity enhancement is expected to be maximized (minimized) when the Néel vector $\boldsymbol{\Delta}$ is perpendicular (parallel) to \mathbf{J}_C . Therefore, the angular dependence measurement of SMR in NM/AFI bilayers can be utilized to determine both the Néel vector and anisotropy constant in AFI.

In an AFM material, the Néel vector will stay along the easy axis below the Néel temperature due to the anisotropy. When applying magnetic field \mathbf{H} parallel to the easy axis with magnitude larger than the critical field H_C , the Néel vector will suddenly change its direction perpendicular to \mathbf{H} , this first-order transition is called spin-flop transition. Since in general cases, the Néel vector in AFM is determined by both the external magnetic

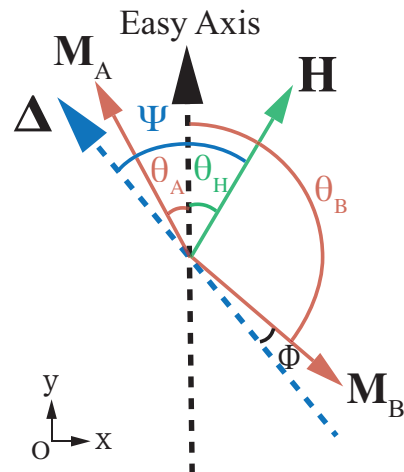


FIG. 2. Schematic for the distribution of the sublattice magnetizations in uniaxial AFI Cr₂O₃(110) thin film and the external magnetic field \mathbf{H} . The easy axis and the Néel vector $\boldsymbol{\Delta}$ in Cr₂O₃(110) are represented with the dashed arrows. The angles relative to the easy axis are labeled with θ_A , θ_B and θ_H . ϕ and ψ represent the tilting angle, the angle between the external field and the Néel vector, respectively.

field and the magnetic anisotropy, a natural question is that if magnetic field \mathbf{H} deviates from the easy axis with angle θ_H , which direction should the AFM Néel vector $\boldsymbol{\Delta}$ point to? Kittel,³² Keffer and Kittel,³³ Nagamiya,³⁴ and others³⁵ have treated the dynamic response of antiferromagnetically coupled sublattices under different magnetic field direction with molecular field approximation, and here we only focus on the static equilibrium condition.

The total magnetic energy of a bulk collinear two-sublattice AFM in an external magnetic field can be phenomenologically written in the following form³⁶:

$$\begin{aligned}
 E_{\text{tot}} &= \int w(\mathbf{M}_A, \mathbf{M}_B) dV \\
 &= \int \{ J \mathbf{M}_A \cdot \mathbf{M}_B - \mathbf{H} \cdot (\mathbf{M}_A + \mathbf{M}_B) + \varepsilon_{\text{ani}} \} dV (1)
 \end{aligned}$$

where \mathbf{M}_i ($i=A, B$), J ($J > 0$), \mathbf{H} and ε_{ani} represent the sublattice magnetization, exchange interaction constant, external magnetic field and magnetic anisotropy energy respectively.

A. Uniaxial AFI Cr₂O₃

In uniaxial AFI Cr₂O₃(110) film, the vectors \mathbf{M}_A , \mathbf{M}_B , \mathbf{H} in Eq. (1) and the corresponding angles θ_A , θ_B , θ_H with the easy axis are illustrated in Fig. 2. ψ is the angle between the external magnetic field and the Néel vector. The magnetic anisotropy energy could be represented as $\varepsilon_{\text{ani}} = -\frac{K}{2}(\cos^2\theta_A + \cos^2\theta_B)$, K ($K > 0$) is the anisotropy constant. In Fig. 2 the external magnetic

field \mathbf{H} can be decomposed into components parallel and perpendicular to Néel vector Δ . The parallel component magnetizes \mathbf{M}_A with changing the magnitude from M_0 to $M_0 + \frac{1}{2}\chi_{\parallel}H_{\parallel}$, here χ_{\parallel} represents parallel susceptibility with $\mathbf{H} \parallel \Delta$. While the perpendicular component drives antiferromagnetic ordered spins to tilt a small angle ϕ from the Néel vector direction, for Cr_2O_3 the angle ϕ is only 1.5° when $\mathbf{H} \perp \Delta$ with magnitude $H \approx 60$ kOe.¹⁹ Assuming the χ_{\parallel}^2 part is negligibly small, we can get the balance of torque equations from Eq. (1), written as³⁵

$$\begin{aligned} (M_0 + \frac{1}{2}\chi_{\parallel}H_{\parallel})H\sin(\psi - \phi) - JM_0^2\sin 2\phi - K\cos\theta_A\sin\theta_A &= 0 \\ (M_0 - \frac{1}{2}\chi_{\parallel}H_{\parallel})H\sin(\psi + \phi) - JM_0^2\sin 2\phi + K\cos\theta_B\sin\theta_B &= 0 \\ \theta_A = \theta_H - \psi + \phi, \theta_B = \theta_H - \psi - \phi + \pi &\quad (2) \end{aligned}$$

Using the relation $2M_0\sin\phi = \chi_{\perp}H_{\perp}$ (χ_{\perp} is the perpendicular susceptibility with $\mathbf{H} \perp \Delta$) and neglecting the $\chi_{\parallel}\chi_{\perp}$ part, the results of Eq. (2) are

$$\chi_{\perp} = \frac{1}{J + (K/2M_0^2)\cos 2(\theta_H - \psi)} \quad (3)$$

$$(\chi_{\perp} - \chi_{\parallel})H^2\sin\psi\cos\psi = K\sin 2(\psi - \theta_H) \quad (4)$$

Eq. (3) can be replaced with a simple formula $\chi_{\perp} = \frac{1}{J}$, since the term $(K/2M_0^2)\cos 2(\theta_H - \psi)$ is usually much smaller than the exchange constant J . Therefore, the perpendicular susceptibility χ_{\perp} is directly related to the exchange constant J (which can be obtained with first-principle calculation³⁷⁻³⁹) through Eq. (3). Define $\theta_{\Delta} \equiv \theta_H - \psi$, and Eq. (4) can be transformed into

$$(\chi_{\perp} - \chi_{\parallel})H^2\sin(\theta_H - \theta_{\Delta})\cos(\theta_H - \theta_{\Delta}) = -K\sin 2\theta_{\Delta} \quad (5)$$

Substituting the parameters in Eq. (5) with the experimental results of susceptibility $\chi_{\parallel} = 1.49 \times 10^{-6}$ emu/g, $\chi_{\perp} = 22.4 \times 10^{-6}$ emu/g and the anisotropy constant $K = 38080$ ergs/g in bulk material Cr_2O_3 ,¹⁹ we plot the $\theta_{\Delta} - \theta_H$ curve under different magnetic field magnitudes, which is shown in Fig. 3(a). The spin-flop field in AFI Cr_2O_3 can be calculated as $H_{\text{SF}} = \sqrt{2K/(\chi_{\perp} - \chi_{\parallel})} \approx 60$ kOe at 300 K. In Fig. 3(a), for $H \ll H_{\text{SF}}$, the Néel vector almost stays along the easy axis with just a small perturbation. And this perturbation of sublattice magnetization becomes stronger with increasing the magnitude of the external magnetic field. Especially for the case when $H \approx H_{\text{SF}}$, the angle of Néel vector θ_{Δ} shows a drastic change when the external magnetic field direction is near the easy axis, since the first order spin-flop transition happens as the magnetic field parallel to the spin axis. While $H \gg H_{\text{SF}}$, the AFM Néel vector follows the external field direction with a relative fixed angle ψ .

With the external field dependent AFM Néel vector, it is easier for us to quantitatively analyze the angular dependent SMR in NM/AFI bilayer under fixed

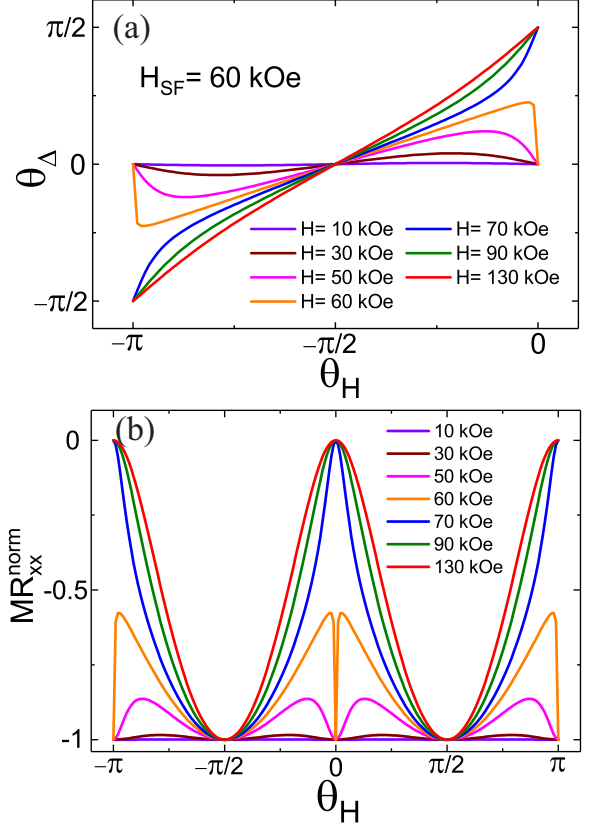


FIG. 3. (a) Simulation curves of the angular dependence of the Néel vector in AFI $\text{Cr}_2\text{O}_3(110)$ thin film with different magnetic fields, and the parameters of the bulk material Cr_2O_3 at 10 K are utilized for the simulation. (b) The external field dependence of the normalized SMR resistivity in $\text{Pt}/\text{Cr}_2\text{O}_3(110)$ are shown with different colors.

magnetic field magnitude. The interface spin current depends on the relative direction of the magnetization and spin accumulation direction, following the formula $(G_r/e)\mathbf{m} \times (\mathbf{m} \times \boldsymbol{\mu}_S)$, where G_r is the interface spin-mixing conductance. \mathbf{m} is the magnetization direction, and $\boldsymbol{\mu}_S$ is the spin accumulation direction at the interface.^{22,23} In the AFI Cr_2O_3 , the interface spin accumulation interacts with both the two sublattice magnetizations \mathbf{M}_A and \mathbf{M}_B . Since the tilting angle ϕ and H_{\parallel} induced magnetization is negligibly small, we can obtain $\Delta = \mathbf{m}_A - \mathbf{m}_B \approx 2\mathbf{m}_A$. The interface spin current can be described as

$$\begin{aligned} (G_r/e)[\mathbf{m}_A \times (\mathbf{m}_A \times \boldsymbol{\mu}_S) + \mathbf{m}_B \times (\mathbf{m}_B \times \boldsymbol{\mu}_S)] \\ = (G_r/e)\mathbf{m}_A \times [(\mathbf{m}_A - \mathbf{m}_B) \times \boldsymbol{\mu}_S] \\ = (G_r/2e)\Delta \times (\Delta \times \boldsymbol{\mu}_S) \end{aligned} \quad (6)$$

where $\mathbf{m}_i = \mathbf{M}_i/M_i$ ($i=A,B$) and Δ represent the sublattice magnetization direction and Néel vector, respectively. In Eq. (6), the AFI Néel vector Δ can substitute

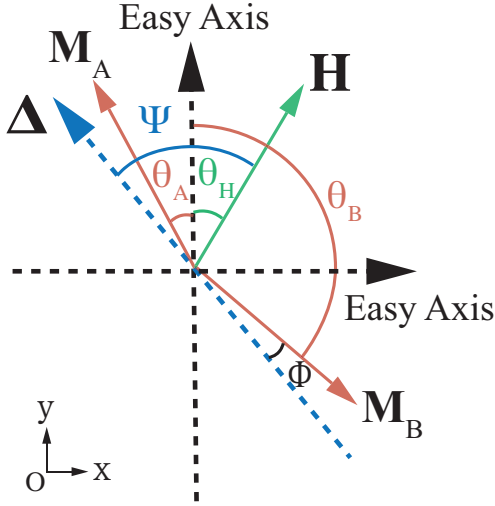


FIG. 4. Schematic for the distribution of the sublattice magnetizations in biaxial AFI NiO(001), CoO(001) thin film and the external magnetic field \mathbf{H} . The two equivalent easy axes and the Néel vector Δ in NiO(001), CoO(001) are represented with the dashed arrows. The angles relative to one of the easy axes are labeled with θ_A, θ_B and θ_H . ϕ and ψ represent the tilting angle, the angle between the external field and the Néel vector, respectively.

for the magnetization direction \mathbf{m} in the FI. Considering the fact that the current induced spin accumulation is polarized along the easy axis (which we define as the \mathbf{y} direction), the longitudinal charge current is modulated as $\mathbf{y} \cdot [\Delta \times (\Delta \times \mathbf{y})]$ and the longitudinal SMR resistivity change is $\rho_{xx} = \rho_{xx0} - \delta\rho_S \Delta_y^2$, $\delta\rho_S$ is the term correlating with the spin mixing conductance and ρ_{xx0} is the resistivity when magnetic field parallel to the easy axis. In a Pt/YIG bilayer, the ratio between the change of resistivity and the resistivity $\delta\rho_S/\rho_{xx0}$ is about 10^{-4} .²² For the comparability of angular dependent SMR under different magnetic fields, it is common to use the normalized longitudinal resistivity, which is defined as

$$\text{MR}_{xx}^{\text{norm}} = \frac{\rho_{xx} - \rho_{xx0}}{\delta\rho_S} = -\Delta_y^2 = -\cos^2(\psi - \theta_H) \quad (7)$$

Figure 3(b) shows the simulated angular dependence of normalized longitudinal resistivity in Pt/Cr₂O₃(110) under different magnetic fields. θ_H is the angle between the easy axis (\mathbf{y} direction) and the magnetic field, as shown in Fig. 2. For $H \ll H_{\text{SF}}$, the curve shows a totally different symmetry with the conventional $\cos^2\theta$ dependence of SMR measured in NM/AFI. As the external field magnitude increases to the spin-flop field, a notable resistance change appears around $\theta_H = 0$, which is also shown in the $\theta_\Delta - \theta_H$ curve, due to the competition between the external magnetic field and magnetic anisotropy. With the magnitude increasing far beyond the spin-flop field $H \gg H_{\text{SF}}$, the SMR curve gradually degenerates into the $\cos^2\theta$ symmetry.

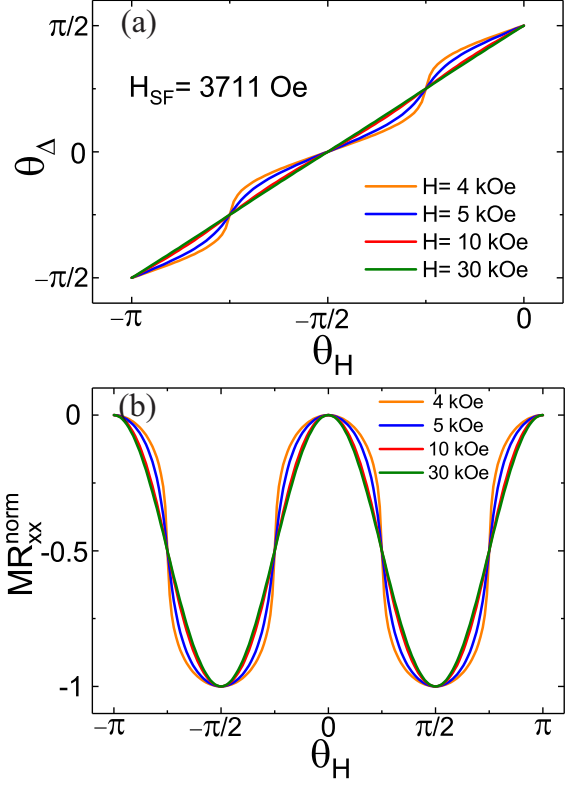


FIG. 5. (a) Simulation curves of the angular dependence of the Néel vector in AFI NiO(001) thin film with magnetic field larger than the spin-flop field, and the parameters of the bulk material NiO at 300 K are utilized for the simulation. (b) The corresponding external field dependence of the normalized SMR resistivity in Pt/NiO(001) are shown with different colors.

B. Biaxial AFI NiO and CoO

For biaxial AFI NiO(001) and CoO(001) films, the magnetic anisotropy energy in Eq. (1) is represented as $\varepsilon_{\text{ani}} = -K \cos 4\theta_\Delta$, and θ_Δ is the angle between Néel vector Δ and one of the anisotropy axis. Figure 4 shows the sublattice magnetization vectors and the applied external magnetic field in NiO(001) and CoO(001) plane. The Néel vector and two equivalent easy axes are represented by the dashed line. We assume the Néel vector initially stays in the (001) surface plane of NiO and CoO. Following the procedure described above, we found that θ_Δ satisfies:

$$(\chi_\perp - \chi_\parallel)H^2 \sin(\theta_H - \theta_\Delta) \cos(\theta_H - \theta_\Delta) = -4K \sin 4\theta_\Delta \quad (8)$$

In a single-crystalline NiO bulk material, the spin-flop field in the (111) plane is given as $H_{\text{SF}} = 4\sqrt{K/(\chi_\perp - \chi_\parallel)}$ = 2400 Oe at 300 K, while the parallel and perpendicular susceptibility are $\chi_\parallel = 6.1 \times 10^{-6}$ emu/g and

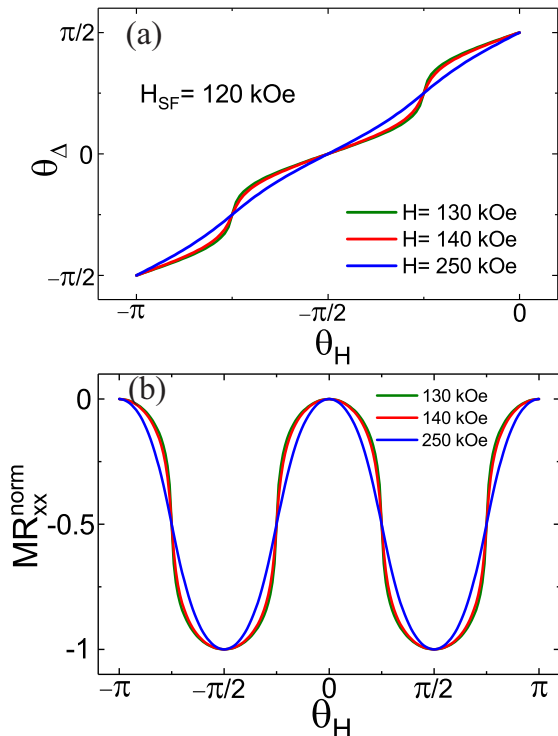


FIG. 6. (a) Simulation curves of the angular dependence of the Néel vector in AFI CoO(001) thin film with magnetic field larger than the spin-flop field, and the parameters of the bulk material CoO at 77 K are utilized for the simulation. (b) The corresponding external field dependence of the normalized SMR resistivity in Pt/CoO(001) are shown with different colors.

$\chi_{\perp} = 12.2 \times 10^{-6}$ emu/g, respectively.⁴⁰ Combining the magnetic torque data obtained in the (001) and (111) plane of single-crystalline NiO²⁶ with the anisotropy constant obtained through the spin-flop field in the (111) plane⁴⁰, we estimate the anisotropy constant in the (001) plane is $K = 5.25$ ergs/g. Substituting the parameters in Eq. (8) with the corresponding values in the NiO(001) plane, we obtain the angular dependence of the Néel vector direction when the external magnetic field rotates in the (001) plane with fixed magnitude, as shown in Fig. 5 (a). When $H \approx H_{SF}$, the distinct bump at the magnetic field direction $\theta_H = \pi/4$ also shows the strong interplay between the external field and anisotropy field. At $H \gg H_{SF}$, the Néel vector Δ almost follows the magnetic field direction with an angle. The angular dependence of the normalized longitudinal resistivity with different field magnitude is shown in Fig. 5 (b). The angular dependence gradually changes to the $\cos^2\theta$ type with increasing the magnitude of the external magnetic field.

In a single-crystalline CoO bulk material, the spin-flop occurs around $H_{SF} = 120$ kOe at 77 K when the external magnetic field is applied along the direction [001].⁴¹ The

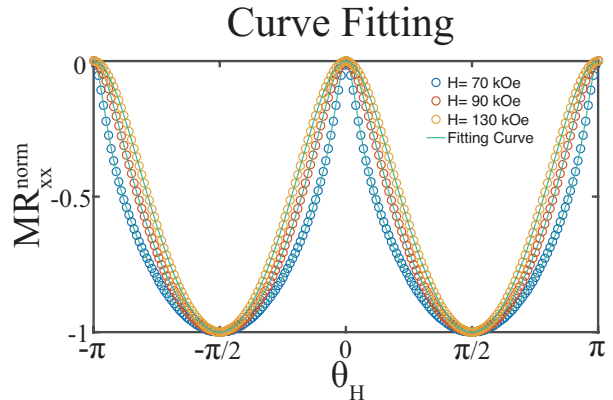


FIG. 7. The fitting curve of the normalized SMR resistivity in Pt/Cr₂O₃(110) at $H > H_{SF}$. The open circles represent the simulation results. And the green solid lines are the fitting curves by only taking the perpendicular susceptibility χ_{\perp} .

corresponding susceptibility values are $\chi_{\parallel} = 3.8 \times 10^{-5}$ emu/g and $\chi_{\perp} = 5.35 \times 10^{-5}$ emu/g respectively. Substituting the parameters in Eq. (8) with the values in the CoO(001) plane, we simulated the $\theta_{\Delta} - \theta_H$ curve in CoO(001) and $MR_{xx}^{norm} - \theta_H$ curve in Pt/CoO(001), which are shown in Figs. 6(a) and (b). The simulation results are qualitatively consistent with the result obtained in NiO(001).

III. SMR RESULTS FITTING

Since the SMR curve in NM/AFI bilayer shows distinctive line shapes under different magnetic fields, it is possible to obtain the anisotropy constant via the SMR curve fitting. Taking the simulated SMR results of Pt/Cr₂O₃(110) as an example, we now try to find out whether the original input parameters could be reproduced through the curve fitting. And the fitting formula is given by combining the Eq. (5) and Eq. (7)³⁵

$$MR_{xx}^{norm} = -\cos^2 \left[\frac{1}{2} \tan^{-1} \left(\frac{\sin 2\theta_H}{\cos 2\theta_H - (\chi_{\perp} - \chi_{\parallel}) H^2 / 2K} \right) - \theta_H \right] \quad (9)$$

where we keep χ_{\perp} as the known parameter. The K and χ_{\parallel} are taken as the fitting parameters. Figure 7 shows the original simulated SMR in Pt/Cr₂O₃ bilayer with $H > H_{SF}$ and a fitting curve. The open circles are the simulation results with the input parameters $\chi_{\parallel} = 1.49 \times 10^{-6}$ emu/g, $\chi_{\perp} = 22.4 \times 10^{-6}$ emu/g, and $K = 38080$ ergs/g. The green solid lines show the fitting with Eq. (9) by only taking the experimental value $\chi_{\perp} = 22.4 \times 10^{-6}$ emu/g. The output fitting parameters are $\chi_{\parallel} = 1.60 \times 10^{-6}$ emu/g, and $K = 37882$ ergs/g, which agrees with the input parameters and proves the feasibility of anisotropy

constant determination through SMR measurement in NM/AFI bilayer.

IV. SUMMARY

In summary, we proposed an electric method for the anisotropy determination in AFIs by using the SMR measurement in NM/AFI bilayer. In both uniaxial and biaxial AFIs, the normalized SMR resistivity in NM/AFI bilayer systems shows different line shapes under different magnetic field magnitudes. Besides, through fitting the results in Pt/Cr₂O₃(110), we obtained the anisotropy constant in Cr₂O₃. This new method paves the way for studying both the Néel vector and anisotropy constant

in both AFI bulk material and thin films.

ACKNOWLEDGMENTS

This work is supported by MOST (Grants No. 2015CB921402), NSFC (Grants No. 11374057, No. 11434003 and No. 11421404), ICC-IMR, Tohoku University, ERATO “Spin Quantum Rectification Project” (No. JPMJER1402) from JST, Japan, Grant-in-Aid for Scientific Research on Innovative Area “Nano Spin Conversion Science” (No. JP26103005) and Grant-in-Aid for young scientists (B) (No. JP17K14331) from JSPS KAKENHI, Japan. T.K. is supported by JSPS through a research fellowship for young scientists (No. JP15J08026).

-
- * dazhi.hou@imr.tohoku.ac.jp
- ¹ T. Jungwirth, X. Marti, P. Wadley, and J. Wunderlich, *Nat. Nanotech.* **11**, 231 (2016).
 - ² S. Seki, T. Ideue, M. Kubota, Y. Kozuka, R. Takagi, M. Nakamura, Y. Kaneko, M. Kawasaki, and Y. Tokura, *Phys. Rev. Lett.* **115**, 266601 (2015).
 - ³ S. M. Wu, W. Zhang, A. KC, P. Borisov, J. E. Pearson, J. S. Jiang, D. Lederman, A. Hoffmann, and A. BhaWutacharya, *Phys. Rev. Lett.* **116**, 097204 (2016).
 - ⁴ T. Shang, Q. F. Zhan, H. L. Yang, Z. H. Zuo, Y. L. Xie, L. P. Liu, S. L. Zhang, Y. Zhang, H. H. Li, B. M. Wang, Y. H. Wu, S. Zhang, and R. W. Li, *Appl. Phys. Lett.* **109**, 032410 (2016).
 - ⁵ D. Hou, Z. Qiu, J. Barker, K. Sato, K. Yamamoto, S. Vélez, J. M. Gomez-Perez, L. E. Hueso, F. Casanova, and E. Saitoh, *Phys. Rev. Lett.* **118**, 147202 (2017).
 - ⁶ W. Lin, K. Chen, S. Zhang, and C. L. Chien, *Phys. Rev. Lett.* **116**, 186601 (2016).
 - ⁷ A. Manchon, *physica status solidi (RRL)* **11**, 1600409 (2017).
 - ⁸ P. Wadley, B. Howells, J. Železný, C. Andrews, V. Hills, R. P. Champion, V. Novák, K. Olejník, F. Maccherozzi, S. S. Dhesi, S. Y. Martin, T. Wagner, J. Wunderlich, F. Freimuth, Y. Mokrousov, J. Kuneš, J. S. Chauhan, M. J. Grzybowski, A. W. Rushforth, K. W. Edmonds, B. L. Gallagher, and T. Jungwirth, *Science* **351**, 587 (2016).
 - ⁹ X. Marti, I. Fina, C. Frontera, J. Liu, P. Wadley, Q. He, R. J. Paull, J. D. Clarkson, J. Kudrnovský, I. Turek, J. Kuneš, D. Yi, J.-H. Chu, C. T. Nelson, L. You, E. Arenholz, S. Salahuddin, J. Fontcuberta, T. Jungwirth, and R. Ramesh, *Nat. Mater.* **13**, 367 (2014).
 - ¹⁰ D. Kriegner, K. Výborný, K. Olejník, H. Reichlová, V. Novák, X. Marti, J. Gazquez, V. Saidl, P. Němec, V. V. Volobuev, G. Springholz, V. Holý, and T. Jungwirth, *Nat. Commun.* **7**, 11623 (2016).
 - ¹¹ C. Hahn, G. de Loubens, V. V. Naletov, J. B. Youssef, O. Klein, and M. Viret, *Europhys. Lett.* **108**, 57005 (2014).
 - ¹² Z. Qiu, J. Li, D. Hou, E. Arenholz, A. T. N’Diaye, A. Tan, K. ichi Uchida, K. Sato, S. Okamoto, Y. Tserkovnyak, Z. Q. Qiu, and E. Saitoh, *Nat. Commun.* **7**, 12670 (2016).
 - ¹³ J. H. Han, C. Song, Y. Y. W. F. Li, G. Y. Wang, Q. H. Yang, and F. Pan, *Phys. Rev. B* **90**, 144431 (2014).
 - ¹⁴ G. R. Hoogeboom, A. Aqeel, T. Kuschel, T. T. M. Palstra, and B. J. van Wees, arXiv:1706.03004.
 - ¹⁵ R. Hölzle, *Magnetismus von Festkörpern und Grenzflächen* (Forschungszentrum Jlich, 1993).
 - ¹⁶ I. Fina, X. Marti, D. Yi, J. Liu, J. Chu, C. Rayan-Serrao, S. Suresha, A. Shick, J. Železný, T. Jungwirth, J. Fontcuberta, and R. Ramesh, *Nat. Commun.* **5**, 4671 (2014).
 - ¹⁷ H.-C. Wu, M. Abid, A. Kalitsov, P. Zarzhitsky, M. Abid, Z.-M. Liao, C. O. Coileáin, H. Xu, J.-J. Wang, H. Liu, O. N. Mryasov, C.-R. Chang, and I. V. Shvets, *Advanced Functional Materials* **26**, 5884 (2016).
 - ¹⁸ U. Gäfvert, L. Lundgren, B. Westerstrandh, and O. Beckman, *J. Phys. Chem. Solids* **38**, 1333 (1977).
 - ¹⁹ S. Foner, *Phys. Rev.* **130**, 183 (1963).
 - ²⁰ V. Beckman, W. Bruckner, W. Fuchs, G. Ritter, and H. Wegener, *phys. stat. sol.* **29**, 781 (1968).
 - ²¹ L. Rebbouh, R. P. Hermann, and F. Grandjean, *Phys. Rev. B* **76**, 174422 (2007).
 - ²² H. Nakayama, M. Althammer, Y. T. Chen, K. Uchida, Y. Kajiwara, D. Kikuchi, T. Ohtani, S. Geprägs, M. Opel, S. Takahashi, R. Gross, G. E. W. Bauer, S. T. B. Goennenwein, and E. Saitoh, *Phys. Rev. Lett.* **110**, 206601 (2013).
 - ²³ A. Brataas, G. E. W. Bauer, and P. J. Kelly, *Phys. Rep.* **427**, 157 (2006).
 - ²⁴ S. Takahashi and S. Maekawa, *J. Phys. Soc. Jpn.* **77**, 031009 (2008).
 - ²⁵ Y. T. Chen, S. Takahashi, H. Nakayama, M. Althammer, S. T. B. Goennenwein, E. Saitoh, and G. E. W. Bauer, *Phys. Rev. B* **87**, 144411 (2013).
 - ²⁶ H. Kondoh, E. Uchida, Y. Nakazumi, and T. Nagamiya, *J. Phys. Soc. Jpn.* **13**, 579 (1958).
 - ²⁷ E. Uchida, N. Fukuoka, H. Kondoh, T. Takeda, Y. Nakazumi, and T. Nagamiya, *J. Phys. Soc. Jpn.* **19**, 2088 (1964).
 - ²⁸ J. E. Hirsch, *Phys. Rev. Lett.* **83**, 1834 (1999).
 - ²⁹ S. O. Valenzuela and M. Tinkham, *Nature* **442**, 176 (2006).
 - ³⁰ J. Sinova, S. O. Valenzuela, J. Wunderlich, C. H. Back, and T. Jungwirth, *Rev. Mod. Phys.* **87**, 1213 (2015).
 - ³¹ E. Saitoh, M. Ueda, and H. Miyajima, *Appl. Phys. Lett.* **88**, 182509 (2006).
 - ³² C. Kittel, *Phys. Rev.* **82**, 565 (1951).
 - ³³ F. Keffer and C. Kittel, *Phys. Rev.* **85**, 329 (1952).

- ³⁴ T. Nagamiya, *Progr. Theoret. Phys. (Kyoto)* **6**, 350 (1951).
- ³⁵ T. Nagamiya, K. Yosida, and R. Kubo, *Advances in Physics* **4**, 1 (1955).
- ³⁶ A. N. Bogdanov, A. V. Zhuravlev, and U. K. Rößler, *Phys. Rev. B* **75**, 094425 (2007).
- ³⁷ A. Filippetti and V. Fiorentini, *Phys. Rev. Lett.* **95**, 086405 (2005).
- ³⁸ M. van Schilfgaarde and V. P. Antropov, *Journal of Applied Physics* **85**, 4827 (1999).
- ³⁹ Z. V. Pchelkina and I. V. Solovyev, *Journal of Physics: Condensed Matter* **27**, 026001 (2015).
- ⁴⁰ E. Uchida, N. Fukuoka, H. Kondoh, T. Takeda, Y. Nakazumi, and T. Nagamiya, *J. Phys. Soc. Jpn.* **23**, 1197 (1967).
- ⁴¹ K. Inagawa, K. Kamigaki, and S. Miura, *J. Phys. Soc. Jpn.* **31**, 1276 (1971).